

Solar constraints on hidden photons re-visited

Javier Redondo^{a,b} and Georg Raffelt^a

^aArnold Sommerfeld Center, Ludwig-Maximilians-Universität, Theresienstr. 37,
80333 München, Germany

^bMax-Planck-Institut für Physik (Werner-Heisenberg-Institut), Föhringer Ring 6,
80805 München, Germany

E-mail: redondo@mpp.mpg.de

Abstract. We re-examine solar emission of hidden photons γ' (mass m) caused by kinetic γ - γ' mixing. We calculate the emission rate with thermal field theory methods and with a kinetic equation that includes γ - γ' “flavor oscillations” and γ absorption and emission by the thermal medium. In the resonant case both methods yield identical emission rates which, in the longitudinal channel, are enhanced by a factor ω_p^2/m^2 (plasma frequency ω_p) in agreement with An, Pospelov and Pradler (2013). The Sun must not emit more energy in a “dark channel” than allowed by solar neutrino measurements, i.e., not more than 10% of its photon luminosity. Together with the revised emission rate, this conservative requirement implies $\chi < 4 \times 10^{-12}(\text{eV}/m)$ for the kinetic mixing parameter. This is the most restrictive stellar limit below $m \sim 3$ eV, whereas for larger masses the transverse channel dominates together with limits from other stars. A recent analysis of XENON10 data marginally improves the solar limit, leaving open the opportunity to detect solar hidden photons with future large-scale dark matter experiments. Detecting low-mass hidden photons with the ALPS-II photon-regeneration experiment also remains possible.

Contents

1	Introduction	1
2	Thermal field theory derivation	3
3	Kinetic Approach	4
4	Emission from the Sun	7
4.1	Resonant emission	7
4.2	Off-resonance production	9
4.3	Solar spectrum	9
4.4	Direct detection of solar HPs	11
5	Other stars	12
6	Production in the Early Universe	13
7	Conclusions	14
8	Acknowledgements	14

1 Introduction

At the low-energy frontier of particle physics [1], the existence of hidden photons (HPs) is an intriguing hypothesis. These particles would have a small mass m and would be completely sterile except for kinetic mixing with normal photons, described by a dimensionless parameter χ . The Lagrangian describing the coupled system is

$$\mathcal{L} = -\frac{1}{4}A_{\mu\nu}A^{\mu\nu} - \frac{1}{4}B_{\mu\nu}B^{\mu\nu} + \frac{m^2}{2}B_\mu B^\mu - \frac{\chi}{2}A_{\mu\nu}B^{\mu\nu}, \quad (1.1)$$

where A and B are the photon and HP fields.

Ongoing experimental searches look for photon appearance from putative HP sources. This includes photon regeneration experiments, beam dump experiments or searches for solar HPs. The usual requirement that stars should not lose excessive amounts of energy in dark channels also leads to restrictive limits [2–6]. HP production in the early universe can be quite efficient despite the small couplings, which makes them excellent candidates for dark matter [7–10] and dark radiation [11] in different parameter ranges. A recent review echoes the various phenomenological aspects of HP models [12].

Returning to stars, it is a peculiarity of HP emission that it depends on density and temperature such that, for small masses, the most restrictive limit arises from the Sun, whereas usually globular cluster stars, white dwarfs, or neutron stars are more constraining.

One way of looking at HP production in a hot medium is γ – γ' oscillations in conjunction with γ absorption and emission, similar to the production of sterile neutrinos in the early universe by active-sterile oscillations. In the stellar plasma, both transverse (T) and longitudinal (L) electromagnetic excitations exist, and both mix with the corresponding HP

polarizations. In a nonrelativistic plasma, L-plasmons have the approximate dispersion relation $\omega = \omega_P$ (plasma frequency) which to lowest order in the small electron velocity does not depend on photon wavenumber k , whereas HPs obey $\omega^2 = m^2 + k^2$. Hence, for any value of ω_P , i.e., at any location in the Sun, there is a population of L-plasmons with the HP wavenumber $k^2 = \omega^2 - m^2$, leading to maximal γ - γ' mixing and thus to resonant emission. This peculiarity of the L dispersion relation makes the L channel important.

As a consequence of the unusual dispersion relation, it is also important to include the non-trivial wave-function renormalization factor in processes with external L-plasmons, corresponding to the correct residue factor of the L-plasmon propagator. In the first calculation of neutrino emission by plasmon decay [13], $\gamma \rightarrow \nu\bar{\nu}$, a superfluous factor K^2/ω^2 was included for L-plasmon decay [14, 15]. Here, $K = (\omega_P, \mathbf{k})$ is the four-momentum of the decaying plasmon. Such incorrect residue factors can easily sneak in, depending on the choice of gauge used in the calculation. Plasmon decay was later extended to relativistic plasmas [16, 17], and once more this factor has crept in (see the remark after Eq. A9 in Ref. [18]). These errors had no practical consequences because, after phase-space integration, the modification was not dramatic and the L-plasmon channel was subdominant anyway.

A similar error in the first calculation of HP emission by one of us [5] once more leads to the same spurious factor K^2/ω^2 , but this time with drastic consequences [6]. This is because here $K^2 = m^2$ for the emitted HP so that the emission rate was underestimated by a factor m^2/ω_P^2 . With $\omega_P \sim 0.3$ keV in the Sun, the correction factor is huge for very low-mass HPs.

While it would be enough to re-scale the previous results with this factor, another aspect of the enhanced emission rate is HP production with keV energies that may be accessible in detectors, but do not correspond to propagating L-plasmons in the Sun. The oscillation mechanism is then not an adequate description. Instead, one may think of the emission, for example, as bremsstrahlung with the electromagnetic field mediating between the electrons and hidden photons in the form of an off-shell propagator [6]. This calculation includes, as a special case, the on-shell production and must reproduce the results from the oscillation approach.

This “propagator approach” simplifies even further if one uses thermal field theory from the start. The calculation of the emission rate then reduces to the almost trivial exercise of reading the expression for the HP thermal self-energy from the Lagrangian Eq. (1.1). The role of the residue factor also becomes immediately obvious.

For on-shell photon-HP conversion, the essential physics is that thermal plasmons oscillate into HPs, collisions with the medium absorb the photon component, destroy the coherence of the mixed state, and in this way produce a population of sterile states that escape. In the “propagator treatment,” oscillations never appear explicitly and one may wonder about its range of validity.

The physics of flavor oscillations combined with collisions is captured in a simple Boltzmann collision equation originally devised for neutrinos [19]. To make connection between the different approaches we also derive HP emission in this picture. In the end we find identical results for the physical circumstances at hand. The crucial condition under which both approaches reconcile is the average flavor conversion between collisions being small. This can happen in two radically different situations: if the mixing angle is small or, even for a large mixing angle, the collisions happen so fast that oscillations do not get far between collisions (strong damping or quantum-Zeno regime). Both conditions are satisfied if the active-sterile “mixing energy” is small compared to the interaction rate of the active quanta. In our case, the mixing energy in the L-channel is $\frac{1}{2}\chi m$. This quantity is extremely small compared

with the relevant L-plasmon absorption rate: we are deeply in the “allowed regime” for the thermal field theory treatment.

2 Thermal field theory derivation

To study the photon–HP system described by the Lagrangian Eq. (1.1), usually the non-orthogonal fields A and B are redefined by $B_\mu = S_\mu - \chi A_\mu$ to introduce the sterile field S_μ . The mixing is thus shifted from the kinetic term to a matrix of mass-squares that mixes the flavors S and A and we find

$$\mathcal{L} = -\frac{1}{4}A_{\mu\nu}A^{\mu\nu} - \frac{1}{4}S_{\mu\nu}S^{\mu\nu} + \frac{m^2}{2}(S_\mu - \chi A_\mu)^2. \quad (2.1)$$

We are interested in small χ and derive our formulas perturbatively in χ . S quanta are produced at order χ^2 , while distinguishing between B and S introduces corrections of order χ^4 so that in practice we may identify S with B .

To obtain the HP emission rate we first observe that the emission rate by a thermal medium for any particle is closely related to the imaginary part of its self-energy Π in the medium. In particular [20]

$$\text{Im } \Pi = -\omega \Gamma, \quad (2.2)$$

where Γ is the rate by which the particle distribution approaches thermal equilibrium. We also consider the absorption rate Γ_{abs} (inverse mean free path) and the spontaneous production rate Γ_{prod} . Detailed balancing reveals $\Gamma_{\text{prod}} = e^{-\omega/T} \Gamma_{\text{abs}}$. Moreover, for bosons $\Gamma = \Gamma_{\text{abs}} - \Gamma_{\text{prod}} = (e^{\omega/T} - 1) \Gamma_{\text{prod}}$. The desired thermal production rate is thus found to be

$$\Gamma_{\text{prod}} = -\frac{\text{Im } \Pi}{\omega (e^{\omega/T} - 1)}. \quad (2.3)$$

We thus seek the imaginary part of the HP self-energy in the medium. At order χ^2 it is given by the graph of Fig. 1 after truncating the external lines. The crosses symbolize the mixing vertex, the internal double line is the thermal photon propagator. Without further ado we find the HP self-energy for a given polarization state to be

$$\Pi_S(K) = m^2 + \chi m^2 \frac{1}{K^2 - \Pi_A(K)} \chi m^2, \quad (2.4)$$

where we use Lorentz gauge and $K = (\omega, k)$ is the four-momentum of the external HP. It fulfills $K^2 = \text{Re } \Pi_S = m^2$ up to corrections of order χ^2 , which disappear in the $m \rightarrow 0$ limit as seen in Eq. (2.4). The real part of the photon self-energy can be taken from the literature. For the imaginary part we can use Eq. (2.2) with Γ_A derived from electron-nucleus bremsstrahlung emission or other processes. The HP production rate thus follows directly from that for ordinary photons.



Figure 1. Self-energy for hidden photons (curly lines) in a thermal medium by mixing with thermal photons of the medium (double line).

In a nonrelativistic plasma, one finds to lowest order in the small electron velocity

$$\text{Re } \Pi_{\text{T}} = \omega_{\text{P}}^2 \quad \text{and} \quad \text{Re } \Pi_{\text{L}} = \frac{K^2}{\omega^2} \omega_{\text{P}}^2. \quad (2.5)$$

The plasma frequency is $\omega_{\text{P}}^2 = 4\pi\alpha n_e/m_e$ with n_e the electron density. Corrections from the electron velocity are of order T/m_e . With $T < 1.3$ keV in the Sun, this is negligible. The corresponding dispersion relations are $\omega^2 - k^2 = \omega_{\text{P}}^2$ for T-plasmons which therefore behave exactly like particles with mass ω_{P} . L-plasmons obey $\omega^2 = \omega_{\text{P}}^2$, independently of wavenumber.

For the L-channel we note that in the denominator $K^2 = Z_{\text{L}}^{-1}\omega^2$ where we define $Z_{\text{L}} = \omega^2/K^2$ so that overall

$$\text{Im } \Pi_{\text{L}}^S = \chi^2 m^4 \text{Im} \frac{Z_{\text{L}}}{\omega^2 - \omega_{\text{P}}^2 - i Z_{\text{L}} \text{Im } \Pi_{\text{L}}^A}. \quad (2.6)$$

We recognize Z_{L} as the residue factor chosen to obtain the canonical pole structure. With $K^2 = m^2$ we have $Z_{\text{L}} = \omega^2/m^2$, explaining the enhanced L-emission noted in Ref. [6].

The residue factor can be interpreted as renormalizing “charges” to which the propagator is attached, here $\chi \rightarrow \sqrt{Z_{\text{L}}} \chi$. This is analogous to $\sqrt{Z_{\text{L}}}$ renormalizing the electron charge in plasmon decay. In the spirit of Eq. (2.2) we must interpret $-Z_{\text{L}} \text{Im } \Pi_{\text{L}}/\omega$ as the damping rate of L quanta, which we denote as Γ_{L} . On the pole of the propagator this is the *physical* damping rate of on-shell L-plasmons. It therefore involves Z_{L} , now renormalizing the electron charge, for example in bremsstrahlung emission.¹

Collecting all factors, we find the HP production rate in the L-channel to be [6]

$$\Gamma_S^{\text{prod}} = \frac{\chi^2 m^2}{e^{\omega/T} - 1} \frac{\omega^2 \Gamma_{\text{L}}}{(\omega^2 - \omega_{\text{P}}^2)^2 + (\omega \Gamma_{\text{L}})^2}. \quad (2.7)$$

Plasmons are weakly damped ($\Gamma_{\text{L}} \ll \omega_{\text{P}}$) so that for $\omega \sim \omega_{\text{P}}$ this is a narrow resonance which, for the purpose of phase-space integration, is a delta function

$$\Gamma_S^{\text{prod}} \sim \frac{\chi^2 m^2}{e^{\omega/T} - 1} \frac{\pi}{2} \delta(\omega - \omega_{\text{P}}). \quad (2.8)$$

Remarkably, for resonant longitudinal HP emission, we do not need any production rate. However, Eq. (2.7) is valid for any ω and thus can be used to compute the emission rate for ω far away from the resonance. In this case one needs $\Gamma_{\text{L}}(\omega) = \Gamma_{\text{L}}(K)|_{K^2=m^2}$ explicitly.

3 Kinetic Approach

Deriving the HP emission-rate in the above form is quick and elegant, but at first glance its equivalence to the flavor oscillation approach may not be entirely obvious. Therefore, we derive the emission rate based on a kinetic equation usually employed in neutrino physics.

We begin with the equation of motion for the mixed fields, which is in Fourier space [5]

$$\left[\omega^2 - k^2 - \begin{pmatrix} \pi(\omega, k) & -\chi m^2 \\ -\chi m^2 & m^2 \end{pmatrix} \right] \begin{pmatrix} A \\ S \end{pmatrix} = 0, \quad (3.1)$$

¹In the original HP emission calculation [5], Z_{L} was correctly included in the damping-rate calculation, but it was overlooked that χ should have been renormalized as well.

where A and S are the field amplitudes. We use the notation $\pi(K) = \text{Re}\Pi(K)$ for the real part of the polarization function which gives us the dispersion relation by virtue of $\omega^2 - k^2 = \pi(\omega, k)$. These equations apply separately to the L and T polarizations.

Oscillating particles are not in propagation eigenstates and thus do not have simultaneously fixed energy and momentum. We here consider evolution in time and thus use quanta of fixed common momentum k . For simplicity we assume relativistic states so that $\omega \approx k$.

For the T case we expand $\omega^2 - k^2 = (\omega - k)(\omega + k) \approx (\omega - k)2k$. After linearizing the equation, we reverse the time Fourier transform, i.e., $\omega \rightarrow i\partial_t$ and find the usual ‘‘Schrödinger equation’’ for flavor oscillations

$$i\partial_t \begin{pmatrix} A(t) \\ S(t) \end{pmatrix} = \begin{pmatrix} \omega_A & \mu \\ \mu & \omega_S \end{pmatrix} \begin{pmatrix} A(t) \\ S(t) \end{pmatrix}. \quad (3.2)$$

Here $\omega_{A,S}$ are the energies of A and S quanta following from the dispersion relation for assumed momentum $k \approx \omega$ and $\mu = -\chi m^2/2k$ is a ‘‘mixing energy.’’

For L-modes the situation is more complicated because the polarization function given in Eq. (2.5) is not simply an effective mass but rather $\pi_L(\omega, k) = \omega_P^2/Z_L$ with $Z_L = \omega^2/K^2$. The Klein-Gordon equation is explicitly

$$\begin{pmatrix} (\omega^2 - \omega_P^2) Z_L^{-1}(K) & -\chi m^2 \\ -\chi m^2 & \omega^2 - \omega_S^2 \end{pmatrix} \begin{pmatrix} A \\ S \end{pmatrix} = 0. \quad (3.3)$$

It is brought to canonical form by $A \rightarrow A/\sqrt{Z_L}$ and $\chi \rightarrow \chi\sqrt{Z_L}$ so that

$$\begin{pmatrix} \omega^2 - \omega_P^2 & -\chi m\omega \\ -\chi m\omega & \omega^2 - \omega_S^2 \end{pmatrix} \begin{pmatrix} A \\ S \end{pmatrix} = 0. \quad (3.4)$$

Linearizing it we recover an oscillation equation of the form Eq. (3.2) with $\omega_A = \omega_P$, $\omega_S = (m^2 + k^2)^{1/2}$, and $\mu = -\chi m/2$. The mixing energy is enhanced by $\sqrt{Z_L}$ in full analogy to the propagator approach.²

The key ingredient for HP production is that flavor oscillations described by this equation are interrupted by collisions and we must understand the evolution of the ensemble, not of individual particles. Therefore, the adequate description is in terms of density matrices. For a fixed momentum \mathbf{k} , the free evolution is described by a Hamiltonian for two coupled harmonic oscillators, $H = \sum_{i,j=A,S} a_i^\dagger \Omega_{ij} a_j$. Here a_i^\dagger and a_i are the creation and annihilation operators, respectively, of quanta with flavor i and

$$\Omega = \begin{pmatrix} \omega_A & \mu \\ \mu & \omega_S \end{pmatrix} = \frac{\omega_A + \omega_S}{2} + \begin{pmatrix} \frac{1}{2}\Delta\omega & \mu \\ \mu & -\frac{1}{2}\Delta\omega \end{pmatrix}, \quad (3.5)$$

where $\Delta\omega = \omega_A - \omega_S$. The ‘‘mixing energy’’ μ is assumed to be small compared to the diagonal elements, causing only a small overall energy modification.

In a kinetic approach, the evolution of the fields A and S is described by the expectation values of field bilinears. In the simplest case, the matrix of occupation numbers $\rho_{ij} = \langle a_j^\dagger a_i \rangle$ captures all relevant information. The field A is assumed to interact with the external medium

²In the original treatment [5], the on-shell value $\pi_L = \omega_P^2 - k^2$ was inserted in Eq. (3.1), representing the correct dispersion relation. However, in this case the external ‘‘charge’’ χ should have been renormalized with $\sqrt{Z_L}$. This error was at least partly caused by the presentation of $\pi_L(\omega, k)$ in Refs. [21, 22] which is only correct on-shell, i.e., for ω and k connected by the dispersion relation. The renormalization factors were separately provided.

by an interaction linear in A , i.e., the medium can absorb or emit A -quanta, but will not scatter them between different momenta. In this case the evolution of different momentum modes is not coupled and the equation of motion for a single momentum mode is [19]

$$\dot{\rho} = -i[\Omega, \rho] + \frac{1}{2}\{G_{\text{prod}}, 1 \pm \rho\} - \frac{1}{2}\{G_{\text{abs}}, \rho\}, \quad (3.6)$$

where $\{\cdot, \cdot\}$ is an anticommutator. The positive sign applies to bosons (Bose stimulation), whereas the negative sign applies to fermions (Pauli blocking). We have defined the matrices

$$G_{\text{prod}} = \begin{pmatrix} \Gamma_{\text{prod}} & 0 \\ 0 & 0 \end{pmatrix} \quad \text{and} \quad G_{\text{abs}} = \begin{pmatrix} \Gamma_{\text{abs}} & 0 \\ 0 & 0 \end{pmatrix}, \quad (3.7)$$

where Γ_{prod} and Γ_{abs} are the production and absorption rates of A -quanta with momentum \mathbf{k} by the medium. In thermal equilibrium they obey $\Gamma_{\text{prod}} = e^{-\omega_A/T} \Gamma_{\text{abs}}$. The commutator part describes flavor oscillations and is equivalent to the earlier Schrödinger equation.

In thermal equilibrium and ignoring flavor oscillations, the S -particles will not be excited at all, whereas the A -particles are thermally occupied according to $f_T = (e^{\omega_A/T} \pm 1)^{-1}$, the negative sign applying to bosons, the positive one to fermions. We then describe a non-equilibrium situation by its deviation from equilibrium in the form

$$\rho = \rho_T + \delta\rho = \begin{pmatrix} f_T & 0 \\ 0 & 0 \end{pmatrix} + \delta\rho. \quad (3.8)$$

The collision term vanishes for ρ_T and we are left with

$$\dot{\rho} = -i[\Omega, \rho] - \frac{1}{2}\{G, \delta\rho\}, \quad (3.9)$$

where $G = \text{diag}(\Gamma, 0)$. The damping rate is $\Gamma = \Gamma_{\text{abs}} \pm \Gamma_{\text{prod}} = (1 \pm e^{-\omega_A/T})\Gamma_{\text{abs}}$. The negative sign is for bosons, i.e., the distribution function approaches equilibrium with the difference between the “spontaneous” absorption and emission rates as mentioned earlier, whereas for fermions (positive sign) it is the sum.

We next write the ρ matrix in terms of occupation number components explicitly

$$\delta\rho = \begin{pmatrix} h_A & g \\ g^* & h_S \end{pmatrix}, \quad (3.10)$$

leading to the equations of motion

$$\dot{h}_A = -\Gamma h_A - 2\mu \text{Im}(g) \quad (3.11)$$

$$\dot{h}_S = 2\mu \text{Im}(g) \quad (3.12)$$

$$\dot{g} = -\left(\frac{1}{2}\Gamma + i\Delta\omega\right)g + i\mu(f_T + h_A - h_S). \quad (3.13)$$

In the absence of damping ($\Gamma = 0$), these equations describe flavor oscillation, in the absence of mixing ($\mu = 0$), the approach of A to thermal equilibrium.

When $\Gamma \gg \mu$ the damping rate is much larger than the oscillation frequency when mixing is maximal for $\Delta\omega = 0$. In other words, on resonance we are in the strong damping regime (quantum Zeno regime), where decoherence between the mixed species is faster than oscillations. When $\Delta\omega$ is sufficiently large, this is no longer the case, but then mixing becomes small. Thus our solution will never stray far from thermal equilibrium, i.e. $|h_A| \ll f_T$ and $|h_S| \ll f_T$.

In this limit, Eq. (3.13) is a closed equation of motion of the form $\dot{g} = -(\frac{1}{2}\Gamma + i\Delta\omega)g + i\mu f_T$. With the initial condition $g(0) = 0$ it has the solution

$$g(t) = \frac{1 - e^{-(i\Delta\omega + \Gamma/2)t}}{\Delta\omega - i\Gamma/2} \mu f_T. \quad (3.14)$$

After an initial transient it approaches the steady-state solution

$$g_\infty = \frac{\Delta\omega + i\Gamma/2}{(\Delta\omega)^2 + \Gamma^2/4} \mu f_T. \quad (3.15)$$

We can now insert this solution into Eq. (3.12), providing us with the steady-state production rate of S quanta,

$$\dot{h}_S = \frac{\Gamma \mu^2}{(\omega_A - \omega_S)^2 + \Gamma^2/4} \frac{1}{e^{\omega_A/T} \pm 1}. \quad (3.16)$$

The only assumption has been that μ is small compared with Γ . Therefore, this solution also applies when many oscillations take place between collisions as long as the oscillation amplitude is small. While oscillations show up in our original transient solution when at $t = 0$ the ensemble had been set up in a pure flavor, they disappear in the steady-state solution which describes the average of the entire ensemble, not individual particles.

We now specialize to the production of longitudinal HPs from the mixing with L-plasmons. Therefore, $\omega_A = \omega_P$, $\Gamma = \Gamma_L$ (damping rate for on-shell L-plasmons) and mixing energy $\mu = -\chi m/2$. For $\omega = \omega_S$ near ω_P this result is identical with Eq. (2.7). However, it is based on the flavor evolution of on-shell L-plasmons and is not applicable for ω very different from ω_P .

4 Emission from the Sun

4.1 Resonant emission

We are here mostly interested in low-mass HPs with $m \ll \omega_P$. Moreover, all over the solar interior we have $\Gamma_L(\omega_P) \ll \omega_P$ and so the HP production is narrowly concentrated around $\omega = \omega_P$ and we may approximate the emission rate as the delta-function of Eq. (2.7). Under this approximation the energy-loss rate per unit volume is

$$Q = \frac{\chi^2 m^2}{e^{\omega_P/T} - 1} \frac{\omega_P^3}{4\pi} \sim \chi^2 m^2 \frac{T \omega_P^2}{4\pi} = \chi^2 m^2 \frac{\alpha T n_e}{m_e}. \quad (4.1)$$

The approximate expression derives from expanding the exponential because L-plasmons are highly occupied (in the solar interior ω_P/T does not exceed 0.23), causing perhaps a 10% overall error.

Integrating the emission rate over the standard solar model AGSS09ph [23] (without expanding the exponential in the emission-rate formula), we find for the HP luminosity in the L-channel

$$L_{S_L} = 5.7 \times 10^{21} \chi^2 \left(\frac{m}{\text{eV}} \right)^2 L_\odot. \quad (4.2)$$

This exotic energy loss is constrained by our relatively precise knowledge of the Sun. The most direct indicators of the properties of the solar interior are the solar neutrino fluxes, and in particular the boron neutrino flux which is especially sensitive to temperature. It has been measured to be $\Phi_{B8}^{\text{meas}} = 5.00(1 \pm 0.03) \times 10^9/\text{cm}^2\text{s}$ (see Table 2 of Ref. [24]). The

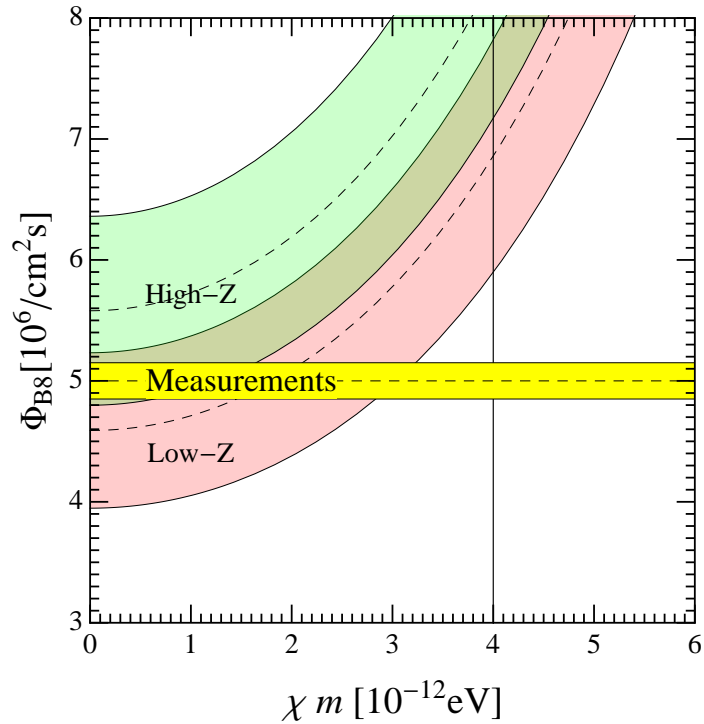


Figure 2. Solar ^8B neutrino flux. *Yellow band:* Measurements. *Red band:* Expectation in the presence of longitudinal HP emission for a solar model with new opacities (low Z). *Green band:* Same for old opacities (high Z). The vertical line corresponds to $L_{SL} < 0.1 L_{\odot}$ (our adopted limit).

presence of some exotic energy loss L_x requires a larger nuclear generation rate and thus an enhanced neutrino flux. It is given to good accuracy by [25, 26]

$$\Phi_{B8}^x = \Phi_{B0}^0 (1 + L_x/L_{\odot})^{4.6}, \quad (4.3)$$

where Φ_{B0}^0 is the flux computed from a solar model unperturbed by exotic losses. In Fig. 2 we show the theoretical expectations for Φ_{B0}^x for two solar models.

The low- Z model (red band) is based on the latest studies of the solar chemical composition [27], which revealed a lower metallicity (lower opacity and thus lower central solar temperature) than previously assumed. It is in slight tension with helioseismology, so for comparison we also show the the high- Z model (green band), i.e., the earlier standard solar model, that fits better helioseismological data. The widths of the bands represent other uncertainties as taken from Table 2 of Ref. [24]. This “solar opacity problem” for the moment remains unresolved. Conceivably, the current abundance of CNO elements in the inner Sun can be determined by future solar neutrino measurements. Ironically, the measured boron neutrino flux (yellow band) lies exactly in the overlap region of the nominal error ranges of the two cases.

Figure 2 suggests $\chi < 3 \times 10^{-12} \text{ eV}/m$ as a limit. Of course, the solar prediction is dominated by systematic issues and an interpretation of the nominal uncertainties in the form of meaningful confidence levels is not available. Therefore, we follow Ref. [26] and adopt the requirement $L_{SL} < 0.1 L_{\odot}$, providing our nominal limit

$$\chi < 4 \times 10^{-12} \frac{\text{eV}}{m}. \quad (4.4)$$

It is shown as a vertical line in Fig. 2. By present evidence, this is a conservative constraint. Conceivably it could be improved in future if the solar opacity problem can be convincingly settled.

4.2 Off-resonance production

Since the L-channel dominates HP emission in at least some range of masses, one may wonder if laboratory experiments could be sensitive to this flux, again caused by HP-photon mixing. These might be more sensitive in the X-ray regime of some keV rather than the sub-keV energies produced by on-shell L-plasmon conversion. Therefore, we compute the expected L-HP spectral flux at Earth for energies above the solar plasma frequency, i.e., for $\omega \gtrsim 0.3$ keV. This will also help us evaluate the solar constraint for HP masses above 0.3 keV.

For this purpose we need the explicit damping rate for L-plasmons which is dominated by inverse bremsstrahlung at low energies and Thomson scattering at high energies. We find explicitly

$$\Gamma_L = \frac{64\pi^2\alpha^3 n_e \sum_Z Z^2 n_Z}{3\sqrt{2\pi} T m_e^{3/2} \omega^3} F\left(\frac{\omega}{T}\right) + \frac{8\pi\alpha^2 n_e}{3m_e^2} \sqrt{1 - \frac{\omega_P^2}{\omega^2}}, \quad (4.5)$$

where n_Z is the density of nuclei of charge Z (in the Sun essentially protons and alpha particles) and

$$F(w) = (1 - e^{-w}) \int_0^\infty dx x e^{-x^2} \int_{\sqrt{x^2+w-x}}^{\sqrt{x^2+w+x}} \frac{t^3 dt}{(t^2 + y^2)^2}. \quad (4.6)$$

Here, $y = k_s/\sqrt{2m_e T}$ with k_s a screening scale, i.e., we model screening by representing the interaction between electrons and nuclei as a Yukawa potential. This approach neglects various other corrections, notably Sommerfeld enhancement, Pauli blocking for partially degenerate electrons and electron-electron bremsstrahlung, which is small in the nonrelativistic limit because of the equal mass of the colliding particles. We also ignore free-bound and bound-bound transitions. Overall we estimate the strike on Γ_L to be at most some 20%.

In the energy range of interest, screening reduces the emission rate at most by a few tens of percent and is partially compensated by other neglected effects. If we ignore screening entirely ($y = 0$), our result agrees with Ref. [6]. In this limit we find analytically

$$F(w) = K_0(w/2) \sinh(w/2), \quad (4.7)$$

where K_0 is a modified Bessel function of the second kind.

It is now straightforward to express the energy-loss rate in terms of Γ_L and integrate over the solar model AGSS09ph [23] for different HP masses. Imposing the earlier constraint $L_{\text{HP}} < 0.1L_\odot$ for the L-channel leads to the constraints marked “Sun-L” in Fig. 3.

For T-modes, exactly the same expressions pertain for Γ_T to lowest order in the electron velocity, in good agreement with Ref. [5]. Integrating over the same solar model and imposing the same constraint leads to the limits marked “Sun-T” in Fig. 3.

4.3 Solar spectrum

For laboratory detection of solar HPs we need the spectral number flux at Earth. The number of HPs emitted in the Sun per unit volume and time is

$$\frac{dN}{dV dt} = \int \frac{d^3\mathbf{k}}{(2\pi)^3} \Gamma_S^{\text{prod}}, \quad (4.8)$$

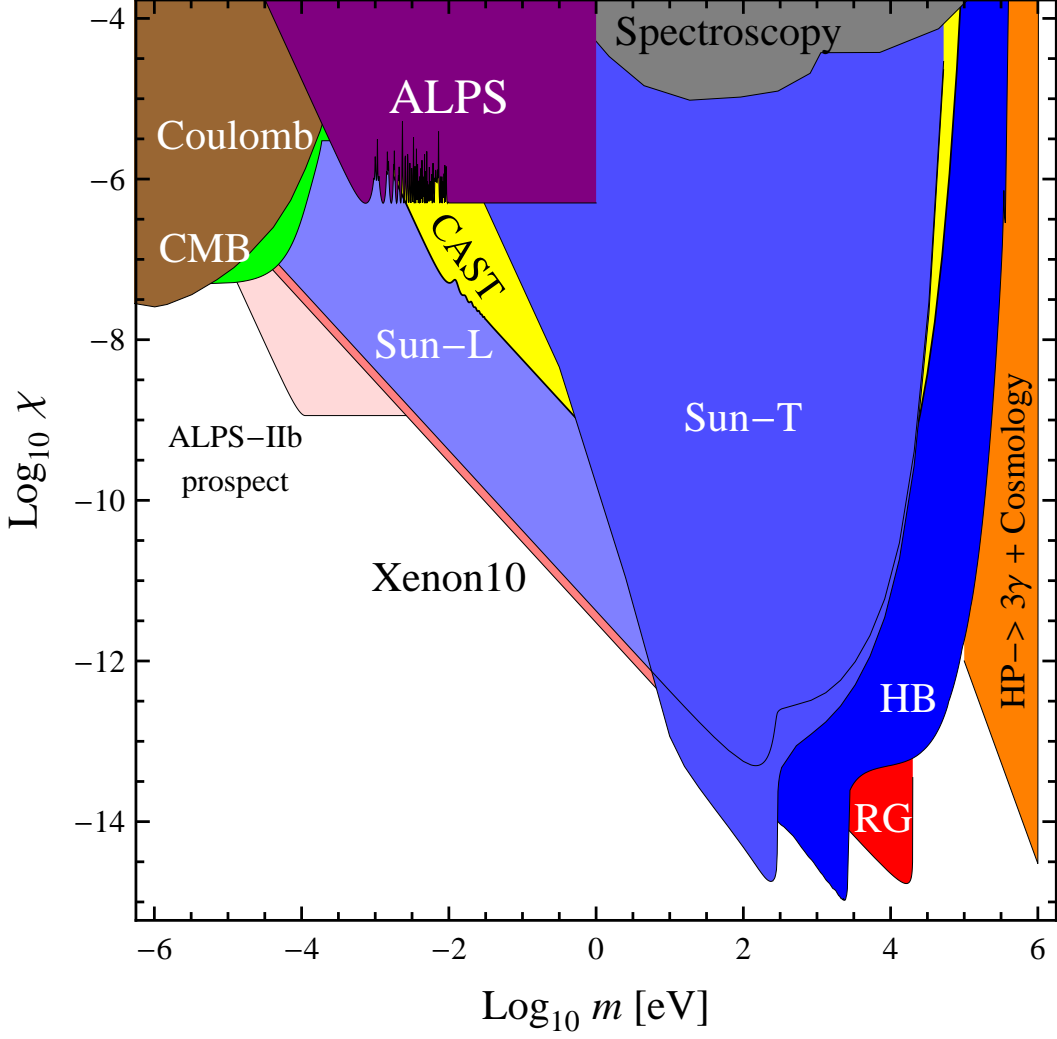


Figure 3. Bounds on hidden photons. The solar energy-loss constraints in the L and T channels as well as the bounds based on horizontal branch (HB) stars and red giants (RG) were derived here. We also show the CAST [5] and recent XENON10 [28] limits on solar HPs (see also [29, 30]) as well as limits from modifications of Coulomb’s law [31], distortions of the CMB spectrum [11], the ALPS photon-regeneration experiment [32], atomic spectroscopy [33] and from decays of relic dark matter HPs [7, 8]. Also shown are prospects for the ALPS-II experiment [34].

whereas the spectral flux at Earth is

$$\frac{d\Phi}{d\omega} = \frac{1}{(1 \text{ AU})^2} \int_0^{R_\odot} dr r^2 \frac{\omega \sqrt{\omega^2 - m^2}}{2\pi^2} \Gamma_S^{\text{prod}}. \quad (4.9)$$

We have performed this integral in the $m \rightarrow 0$ limit by using the solar model AGSS09ph [23] and obtain the flux shown in Fig. 4. We have included a screening correction to bremsstrahlung based on the Debye scale including both electrons and ions, causing a barely visible modification on the scale of this plot.

The emission is dominated by energies below the maximum solar $\omega_p \sim 0.3 \text{ keV}$ where the production is resonant. The energy dependence of this resonant flux can be explored by

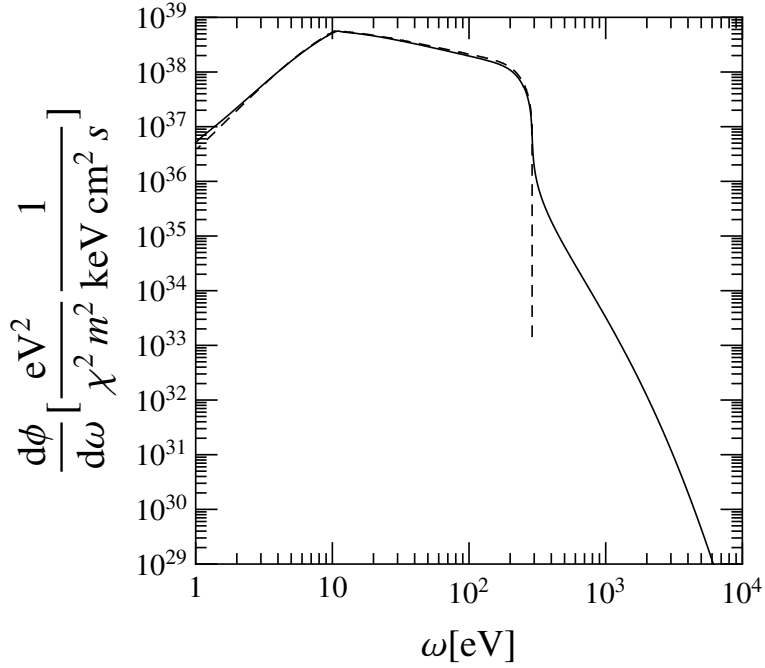


Figure 4. Flux at Earth of L-HPs in the limit $m \rightarrow 0$. For non-zero masses multiply with $\sqrt{1 - m^2/\omega^2}$. The dashed line is the resonant flux based on the analytic arguments described in the text.

using Eq. (2.8) to perform the r integration. Thus using $\Gamma_S^{\text{prod}} \propto \delta[\omega - \omega_P(r)]$ yields

$$\frac{d\Phi}{d\omega} \approx \frac{\chi^2 m^2}{(1 \text{ AU})^2} \frac{r_\omega^2 T_\omega}{2\pi^2} \left| \frac{d \log \omega_P^2(r)}{dr} \right|_{r=r(\omega)}^{-1}, \quad (4.10)$$

where r_ω and T_ω are the values of the radius and temperature where $\omega_P = \omega$. We have plotted this contribution as a dashed line in Fig. 4. Low energies correspond to emission regions near the solar surface whereas $\omega \rightarrow 0.3$ keV corresponds to the solar center. The analytical formula describes well the numerical results, including the break at $\omega \sim 10$ eV, which originates from the electron density dropping much faster near the surface.

Energies $\omega \gtrsim 0.3$ keV cannot be produced resonantly and the flux reduces considerably. An approximation formula for the flux at Earth in this range is

$$\begin{aligned} \frac{d\Phi}{d\omega} &= \chi^2 m^2 5.7 \times 10^{33} \text{ cm}^{-2} \text{ s}^{-1} \text{ keV}^{-1} \\ &\times \left[1 + \frac{0.002}{(\omega - 0.28)^{1.8}} \right] \omega^{-4} e^{-\omega/1.7}, \end{aligned} \quad (4.11)$$

where m is in eV and ω in keV. The accuracy is better than 10% for $0.3 \text{ keV} < \omega < 11 \text{ keV}$. The strong suppression at high energies comes from the suppression of the mixing by medium effects and the ω^{-3} dependence of the bremsstrahlung rate. Above a few keV, the spectrum is exponentially suppressed.

4.4 Direct detection of solar HPs

The solar HP flux may be detectable in laboratory experiments. In the T-channel, the CAST experiment provides the most restrictive limit for sub-eV mass HPs (yellow region in Fig. 3).

However, the T-channel flux is maximum at eV energies where the most sensitive CAST detectors are blind. Experiments aiming at \sim eV HPs have already been performed by CAST [35], SUMICO [29] or are taking data (SHIPS [36]) but their constraining power is limited until a solid estimate of the low energy T-channel flux is available (see also [37, 38]).

In the L-channel, large-scale dark matter detectors can be sensitive by virtue of the inverse processes that produce HPs in the Sun [28]. At present, only the XENON10 experiment appears to have any meaningful sensitivity. According to Ref. [28], the absence of excess counts above background implies a limit $\chi < 3 \times 10^{-12}$ eV/ m , identical with the solar energy-loss limit suggested by our Fig. 2 and slightly more restrictive than our adopted conservative limit. In other words, dark matter detectors are only beginning to probe solar HPs, leaving open the possibility that future larger-scale instruments could actually find solar HPs.

5 Other stars

To compare the impact of L-HP emission on stars other than the Sun, it is easier to compare the usual energy-loss rate per unit mass. We first focus on small HP masses for which some analytical insight can be provided. The mass density is ρ and the electron density is approximately $n_e = Y_e \rho / m_p$, where Y_e is the number of electrons per baryon (1 for hydrogen, 0.5 for helium, carbon, and oxygen). For small m , Eq. (4.1) leads to

$$\varepsilon = \frac{Q}{\rho} \sim \chi^2 m^2 \frac{\alpha}{m_e m_p} Y_e T. \quad (5.1)$$

Essentially ε depends only on temperature T .

Besides the Sun, one may consider HP emission from the non-degenerate helium-burning cores of horizontal-branch (HB) stars in globular clusters that usually provide more restrictive constraints than the Sun, for example on axion emission. In the Sun, a typical T is 1 keV, in the cores of HB stars 8 keV. (Helium burns at higher temperature than hydrogen.) $Y_e = 0.5$ in HB-star cores, in the Sun more like 0.8. In the Sun, the average nuclear energy generation rate is around $2 \text{ erg g}^{-1} \text{ s}^{-1}$, whereas in the helium-burning HB core it is around $80 \text{ erg g}^{-1} \text{ s}^{-1}$. In both cases, energy loss into a “dark channel” is constrained to be less than some 10% of ε_{nuc} . In other words, the constraint on HP emission from the Sun would be roughly a factor of 10 more restrictive. This unusual result arises from ϵ_{HP} not depending on density at all and on temperature only linearly.

However, for HP masses exceeding a few keV, the emission from the Sun is thermally suppressed, providing a window where HB stars still provide a useful limit. We have computed the HP luminosity (in L and T modes) of a typical HB star (see Fig. 2.4 of Ref. [22], taken from Ref. [42]) for different HP masses. Imposing the HP luminosity to be smaller than 10%, we obtain the constraint “HB” shown in Fig. 3.

For yet larger HP masses, the higher density of more evolved stars allows for resonant production. Red-giant stars before He ignition probably provide an opportunity because in their degenerate core the plasma frequency reaches $\omega_p \sim 20 \text{ keV}$ at $T \sim 8.6 \text{ keV}$. Imposing that the energy-loss rate in L-HPs is smaller than $10 \text{ erg g}^{-1} \text{ s}^{-1}$ as suggested in [22, 39–41] we obtain from Eq. (4.1) the exclusion region “RG” depicted in red in Fig. 3.

For HP masses larger than 20 keV, we would need well studied stars denser than RG cores before Helium ignition to produce HPs resonantly, but no standard argument seems to be available.

6 Production in the Early Universe

In the low-mass region, the production of L HPs in the Sun overshadows the production of T modes. It is reasonable to ask whether this is also the case for the relic HPs produced in the big bang, where L-modes were neglected in previous works [7, 8, 11], at least partially due to the mentioned error in the solar L-emission rate [5]. An, Pospelov and Pradler have already argued that L-modes are not copiously produced in the early universe [6] and we agree with their arguments. Still, it is instructive to provide a simple quantitative estimate. Since HPs with $m > 2m_e$ decay very efficiently into three photons, they require extremely small χ -values to be cosmologically stable and we prefer to focus on $m < 2m_e$.

The production of relic L-HPs follows neatly from our derivations above. In particular, Eq. (2.7) holds because the Hubble expansion is slow and thermal equilibrium is always a good approximation. We define the usual comoving momentum as $k_c = ka$, with $a = a(t)$ the scale factor. The phase-space distribution of relic L HPs is given by integrating in time the production rate as

$$f(k_c) = \int_0^{t_0} \Gamma_S^{\text{prod}}(\omega, k_c/a) dt, \quad (6.1)$$

where $\omega = \sqrt{(k_c/a)^2 + m^2}$.

When $T \gtrsim m_e$, electrons and positrons are relativistic and Π_A has to be modified. However, even in this case it has similar properties: $\text{Re } \Pi = m_\gamma^2 \simeq \omega_P^2$ and $\text{Im } \Pi \ll \text{Re } \Pi$. The exact form is not relevant. The production of HPs with a given present-day momentum k_c is dominated by the resonance, i.e., when $\omega = m_\gamma \simeq \omega_P$ and the ambient on-shell L-plasmons can oscillate into L-HPs. This simplifies the calculation, providing

$$f_L(k_c) \approx \chi^2 \frac{\pi}{j(T)} \frac{m^2 T}{\omega^2 H} \Big|_{\text{res}} \quad (6.2)$$

where we have used $\exp(\omega/T) \sim \omega/T$. The Hubble factor is $H = a^{-1} da/dt$ and $j(T) = d \log \omega_P^2 / d \log a \sim O(1)$ [8]. On the RHS, ω , H and T have to be evaluated at the resonance.

The frequency dependence is $\sim T/\omega^2 H$, which strongly decreases with ω (earlier resonances). Momenta with $k < m$ convert when $\omega_P = \omega \simeq m$ and go through the resonance almost simultaneously. These HPs are thus created non-relativistically and constitute a form of dark matter. (They decouple after the resonance if their mixing is small such that indeed only the resonance produces them efficiently.)

The analogous relic density of transverse HPs is [8]

$$f_T(k_c) \approx \chi^2 \frac{\pi}{j(T)} \frac{m^2}{HT} \left[\frac{T}{\omega} \frac{1}{e^{\omega/T} - 1} \right] \Big|_{m=\omega_P}. \quad (6.3)$$

They feature an almost thermal spectrum and are produced resonantly when $\omega_P = m$, i.e., almost simultaneously with L-modes. The abundance involves the evaluation of H, T, j at the same moment as L-modes so we can express our results as a ratio of densities,

$$\frac{n_L}{n_T} \simeq \frac{1}{\pi^2} \frac{m}{T_{\text{res}}}. \quad (6.4)$$

This ratio is always small because $m = \omega_P$ is suppressed with respect to T at least by the electron charge. We conclude that the dark matter or dark radiation in L-modes is always smaller than in T-modes. As anticipated, the earlier DM estimates based on T-modes alone [8] do not change significantly for $m < 2m_e$.

7 Conclusions

We have revisited solar emission of hidden photons. A previous calculation by one of us [5] had missed a crucial wave-function renormalization factor as correctly pointed out by An, Pospelov and Pradler [6]. We have derived the emission rate in terms of the imaginary part of the in-medium HP self-energy in the spirit of thermal field theory, similar to the approach chosen in Ref. [6], and using a kinetic approach, closer to the picture of active-sterile flavor oscillations with collisions, similar to the original approach of Ref. [5]. In the resonant case, where ambient on-shell L-plasmons convert to L-HPs, both results are identical. For HP energies ω exceeding the plasma frequency, resonant production is not possible and one needs the thermal field theory approach.

We have updated several stellar energy-loss and cosmological limits, but the only tangible change occurs for $m < 3$ eV where the most restrictive limit among all astrophysical arguments arises from solar L-mode emission. The measured ^8B neutrino flux tightly constrains the solar interior temperature and therefore the allowed range of invisible energy losses L_x . Based on a generous upper limit of $L_x < 0.1 L_\odot$ we have derived a new limit on the kinetic mixing parameter given in Eq. (4.4) and shown in Fig. 3 marked “Sun-L.”

In future, large-scale dark-matter detectors may be able to find solar HPs which cause ionization by bound-free transitions in the detector material. At present, only XENON10 is marginally sensitive to the solar flux and provides a constraint similar to the one derived from the solar neutrino flux [28]. Therefore, future large-scale dark matter detectors have the opportunity to detect solar HPs—any increase in sensitivity explores uncharted territory in parameter space. Likewise, the photon regeneration experiment ALPS-II, a pure laboratory approach, will explore a region of low-mass HP parameter range that is apparently not accessible by any other method.

8 Acknowledgements

We thank Alexander Kartavtsev for informative discussions about thermal field theory. We acknowledge partial support by the Deutsche Forschungsgemeinschaft through grant No. EXC 153 and by the European Union through the Initial Training Network “Invisibles,” grant No. PITN-GA-2011-28944. J.R. acknowledges support by the Alexander von Humboldt Foundation.

References

- [1] J. Jaeckel and A. Ringwald, *Ann. Rev. Nucl. Part. Sci.* **60**, 405 (2010), arXiv:1002.0329.
- [2] L. B. Okun, *Sov. Phys. JETP* **56**, 502 (1982) [*Zh. Eksp. Teor. Fiz.* **83**, 892 (1982)].
- [3] V. V. Popov and O. V. Vasil’ev, *Europhys. Lett.* **15**, 7 (1991).
- [4] V. Popov, *Turkish Journal of Physics* **23**, 943 (1999).
- [5] J. Redondo, *JCAP* **0807**, 008 (2008), arXiv:0801.1527.
- [6] H. An, M. Pospelov and J. Pradler, arXiv:1302.3884.
- [7] M. Pospelov, A. Ritz and M. B. Voloshin, *Phys. Rev. D* **78**, 115012 (2008), arXiv:0807.3279.
- [8] J. Redondo and M. Postma, *JCAP* **0902**, 005 (2009), arXiv:0811.0326.
- [9] A. E. Nelson and J. Scholtz, *Phys. Rev. D* **84**, 103501 (2011), arXiv:1105.2812.

- [10] P. Arias, D. Cadamuro, M. Goodsell, J. Jaeckel, J. Redondo and A. Ringwald, JCAP **1206**, 013 (2012), arXiv:1201.5902.
- [11] J. Jaeckel, J. Redondo and A. Ringwald, Phys. Rev. Lett. **101**, 131801 (2008), arXiv:0804.4157.
- [12] J. Jaeckel, arXiv:1303.1821.
- [13] J. B. Adams, M. A. Ruderman and C. -H. Woo, Phys. Rev. **129**, 1383 (1963).
- [14] V. N. Tsytovich, JETP **45**, 1183 (1963) [Sov. Phys. JETP **18**, 816 (1964)].
- [15] M. H. Zaidi, Nuovo Cim. A, **40**, 502 (1965).
- [16] E. Braaten, Phys. Rev. Lett. **66**, 1655 (1991).
- [17] N. Itoh, H. Mutoh, A. Hikita and Y. Kohyama, Astrophys. J. **395**, 622 (1992); Erratum ibid. **404**, 418 (1993).
- [18] E. Braaten and D. Segel Phys. Rev. D **48**, 1478 (1993), hep-ph/9302213.
- [19] G. Sigl and G. Raffelt, Nucl. Phys. B **406**, 423 (1993).
- [20] H. A. Weldon, Phys. Rev. D **28**, 2007 (1983).
- [21] M. Haft, G. Raffelt and A. Weiss, Astrophys. J. **425**, 222 (1994); Erratum ibid. **438**, 1017 (1995), astro-ph/9309014.
- [22] G. G. Raffelt, *Stars as Laboratories for Fundamental Physics* (University of Chicago Press 1996).
- [23] A. Serenelli, S. Basu, J. W. Ferguson and M. Asplund, Astrophys. J. **705** L123 (2009), arXiv:0909.2668.
- [24] W. C. Haxton, R. G. Hamish Robertson and A. M. Serenelli, Annu. Rev. Astr. Astrophys. **51**, in press (2013), arXiv:1208.5723.
- [25] H. Schlattl, A. Weiss and G. Raffelt, Astropart. Phys. **10**, 353 (1999), hep-ph/9807476.
- [26] P. Gondolo and G. Raffelt, Phys. Rev. D **79**, 107301 (2009), arXiv:0807.2926.
- [27] M. Asplund, N. Grevesse, A. J. Sauval and P. Scott, Ann. Rev. Astron. Astrophys. **47**, 481 (2009), arXiv:0909.0948.
- [28] H. An, M. Pospelov and J. Pradler, arXiv:1304.3461.
- [29] T. Mizumoto, R. Ohta, T. Horie, J. Suzuki, Y. Inoue and M. Minowa, arXiv:1302.1000.
- [30] R. Horvat, D. Kekez, M. Krčmar, Z. Krečak and A. Ljubičić, Phys. Lett. B **721**, 220 (2013), arXiv:1210.1043.
- [31] D. F. Bartlett, P. E. Goldhagen and E. A. Phillips, Phys. Rev. D **2**, 483 (1970).
- [32] K. Ehret *et al.*, Phys. Lett. B **689**, 149 (2010), arXiv:1004.1313.
- [33] J. Jaeckel and S. Roy, Phys. Rev. D **82**, 125020 (2010), arXiv:1008.3536.
- [34] R. Bähre *et al.*, arXiv:1302.5647.
- [35] G. Cantatore *et al.* [CAST Collaboration], Nucl. Instrum. Meth. A **617** (2010) 502.
- [36] M. Schwarz, *et al.*, arXiv:1111.5797.
- [37] S. N. Gninenko and J. Redondo, Phys. Lett. B **664**, 180 (2008), arXiv:0804.3736.
- [38] J. Redondo, arXiv:1202.4932.
- [39] G. G. Raffelt, Astrophys. J. **365**, 559 (1990).
- [40] G. Raffelt and A. Weiss, Phys. Rev. D **51**, 1495 (1995), hep-ph/9410205.
- [41] M. Catelan, J. A. de Freitas Pacheco and J. E. Horvath, Astrophys. J. **461**, 231 (1996),

astro-ph/9509062.

[42] D. Dearborn, G. Raffelt, P. Salati, J. Silk and A. Bouquet, *Astrophys. J.* **354**, 568 (1990).